

**Referee comments:** The paper entitled “Multiscale effects caused by the fracturing and fragmentation of rock blocks in rock mass movement: Implications for rock avalanche propagation” reports a study on the relation between fracturing and fragmentation of sliding blocks and the propagation features of rock avalanches. The work is scientifically interesting; nevertheless, I have some criticism as commented in the following.

First of all, I suggest some corrections pertaining to the use of the English language.

Thank you for your suggestion. After the revision, to further correct the English usage, grammar, and sentence structure, we will ask an English editing service to polish our revised manuscript.

**Referee comments:** I also suggest the authors to describe rock avalanches in a more “geomorphic” way in Ch.1 - Introduction; in this regard I suggested some literature references.

Thank you very much for your kindly suggestions. According to the references proposed by the referee, this sentence and the following sentence are rewritten as “Rock avalanches are extremely rapid, massive, flow-like motion of fragmented rock from large rockslides and rockfalls, which experiencing intense disintegration and fragmentation (Knapp and Krautblater, 2020; Hungr et al., 2014; McSaveney and Davies, 2006). They can effectively shape mountainous landscapes (Lucas et al., 2014; Crosta et al., 2018; Francioni et al., 2019; van Wartburg et al., 2020), and have also caused several casualties and large economic losses in recent decades due to their extremely long travel distances (Heim, 1932; Evans et al., 2007, 2009; Fan et al., 2017; Zhang et al., 2021; Shugar et al., 2021).”

**Referee comments:** Anyhow, the major issues concern the adopted methodology. In particular, I suggest to better explain some steps (e.g. line 152 – The gravitational acceleration ( $g'$ ) is enhanced to  $1962\text{ m/s}^2$  (200 g) to mimic the real stress field) based on literature data or other sources you considered. In this way, the comprehensibility of the whole work would surely be enhanced.

Thank you very much for your insightful suggestions.

First of all, the choice of gravitational acceleration ( $g'$ ) in DEM model is according to Zhao et al. (2017, 2018). In the initial Manuscript, we cited them at the previous sentence as shown in Lines 151-152. Therefore, for better explanation, we cited the references in this sentence in the revised Manuscript. When the gravitational acceleration is 200 g, the stress level in the DEM model is similar to the real stress field of rock avalanche.

In order to better explain some steps in DEM model and enhance the comprehensibility of the whole work, we modified the structures of Section 2 “DEM model setup”. And add more information about the setup of DEM model. The following paragraphs attached the new version of Section 2:

Previous studies have proven that DEM models can successfully simulate the dynamic behavior of dry granular flows (Silbert et al., 2001; Bi et al., 2005; Morgan and McGovern, 2005; Utili et al., 2015; Kermani et al., 2015; Lai et al., 2017), crack nucleation and propagation of rock blocks under different loading rates (Yoon 2007; Wang and Tonon, 2011; Shen et al., 2017; Ma et al., 2018) and the fragmentation process of rock avalanches (Thompson et al., 2010; Lo et al., 2011; Li et al., 2012; Deng et al., 2016; Zhao and Crosta, 2018). Therefore, the commercial DEM software particle flow code in two dimensions (PFC2D) is employed to run all of the simulations discussed here (Cundall, 1971; Cundall and Strack, 1979).

In PFC2D, the basic element is a disc, and granular material is simulated as an assembly of discs. By using force-displacement law to update the position and force of each particle (disc), and using Newton’s second law to determine the motion of each particle, then the behavior of a granular flow can be determined by the motion and interaction of particle aggregates. DEM employ a time-step algorithm to update the position and force of each particle, the macroscopic kinetics of the particle aggregates are determined based the continuous accumulation of force and displacement at each time step (Lin et al., 2020b). In general, rock blocks are modeled as cemented tightly packed discs (particles) via a linear parallel bond model (consists of a linear model and a parallel-bond model, Fig. 1a), presenting brittle fracture characteristics as the bonds instantly break and disappear once the force acting on the bond reaches the failure criterion (Potyondy and Cundall, 2004). After the bond breaks, the interaction between dispersed particles is replaced by a linear model (the parallel-bond model vanished and the linear model sustained, Fig. 1b), in which the motions of particles and blocks are controlled by Newton’s second law of motion. Therefore, dynamic fragmentation can be well simulated by this bonded-particle model (Zhao et al., 2017, 2018).

In the lineal parallel bond model, the interaction of two discs can be described as (Potyondy and Cundall, 2004):

$$F_c = F_l + F_b \quad (1)$$

$$M_c = M_b \quad (2)$$

$$F_l = K_{n1}g_n + F_s^{i-1} + K_{s1}\Delta g_s \quad (3)$$

$$F_b = K_{n2}(d - d_0) + K_{s2}\Delta g_s \quad (4)$$

$$M_b = K_{n3}\Delta g_b \quad (5)$$

where  $F_c$  is the contact force,  $F_l$  is the linear force in the linear model,  $F_b$  is the parallel-bond force.  $M_c$  and  $M_b$  are the contact moment and the parallel-bond moment, respectively. As the linear model component does not resist

relative rotation, the  $M_c$  is always equal to the moment carried by the parallel bond model component ( $M_b$ ).  $F_l$  consists of the normal force and the shear force in the linear model component. The normal force is calculated as the normal stiffness of contact in the linear model ( $K_{nl}$ ) times the overlapping distance between two discs ( $g_n$ ) in contact. The shear force is calculated as the shear stiffness of contact in the linear model ( $K_{sl}$ ) times the incremental shear displacement ( $\Delta g_s$ ) and add the shear force calculated at the previous time step ( $F_s^{i-1}$ ). Likewise,  $F_b$  consists of the normal force and the shear force in the parallel-bond model component.  $K_{n2}$  and  $K_{s2}$  are the corresponding bond stiffness in the normal and shear directions, respectively,  $d$  and  $d_0$  are the current and initial distances of two discs. The parallel-bond moment ( $M_b$ ) is resolved into a twisting and bending moment, while the twisting moment is equal to 0 in the 2D model. Thus, the contact moment ( $M_c$ ) is always equal to the bending moment carried by parallel-bond model, which expressing as the bond stiffness in the bending direction ( $K_{n3}$ ) times the relative displacement between bonded discs in the bending direction ( $\Delta g_b$ ). More details related to contact models and the basic theories of DEM can be found in Itasca (2014).

After macrocracks develop during fragmentation in the rock mass, only the elastic strain energy carried by the bond vanishes; meanwhile, the remaining elastic strain energy stored in unbroken bonds and the overlap deformation of particles will still transform, accumulate and release. This process provides exceptional opportunities to observe and analyze the conversion of elastic strain energy during the fragmentation process in the transport of brittle materials during the movement of fragmentable blocks (Potyondy and Cundall, 2004; Timar et al., 2012; Shen et al., 2017; Gao et al., 2020, 2021).

A schematic view of the model configuration is shown in Fig. 2. The traveling path of a rectangular rock block is mainly composed of an inclined slope and a horizontal plane. An arc connection path with a radius of 0.1 m is added between two planes. The inclined plane in the traveling path is a frictionless rigid one with a slope angle of  $30^\circ$ , while the friction angle of the arc and horizontal planes is  $30^\circ$  to dissipate kinetic energy. Similar to Zhao et al. (2017, 2018) and Bowman et al. (2012), the size of the rock block is  $94 \text{ mm} \times 45 \text{ mm}$ , which consists of 11812 particle aggregates cemented by the parallel-bond model. Choosing the microparameters of the rock block in DEM model is based on the numerical procedure applied in Potyondy and Cundall (2004), in which the macroproperties of Lac Du Bonnet granite (Martin, 1993) are used. Uniaxial compressive tests and uniaxial tensile tests are employed to calibrate the microparameters of rock block in the simulation. The input values of microscopic parameters in the DEM model are selected by trial and error to ensure that the mechanical characteristics of the rock block in the simulation match those of the real Lac Du Bonnet granite. Table 1 shows the input microparameter values of the DEM model. The uniaxial compressive strength, Young's modulus, Poisson's ratio and tensile strength of the rock

block in the simulation are 200.4 MPa, 67.6 GPa, 0.259 and 40.97 MPa, respectively. The drop height of rock block ( $H$ ) in this simulation is 0.12 m. The gravitational acceleration ( $g'$ ) is enhanced to  $1962 \text{ m/s}^2$  ( $200g$ ) to mimic the approximately real stress field for rock avalanches (Zhao et al., 2017, 2018).

For 2D DEM simulations, which differ from the traditional plane strain or plane stress situation, there are no direct laboratory experimental results that can be used for the calibration of damping values (energy dissipation by the interaction of particles and between particle and boundary). Based on our previous 3D DEM simulation and other similar simulations (Giani et al. 2004; Lo et al., 2014; Murugaratnam et al. 2015; Lin et al., 2020a), the local, normal, and shear viscous damping terms are set to 0.06, 0.36, and 0.11, respectively. Note that viscous damping affects only the efficiency of energy dissipation and the eventually runout distance of sliding blocks (Johnson et al., 2016); the dynamics of the block system and the fragmentation mechanism of the rock block are not changed. Each simulation shows a typical rock fracturing and emplacement process, which validates the applicability of these microparameters for the DEM model.

Joints with different strengths and numbers are predesigned in the rock blocks. The inset table in Fig. 2 gives the forms and parameters of predesigned joints. T1, T2 and T3 represent a rock block with one joint, which varies in the tensile strength of the joint. T4, T5 and T6 represent a rock block with two joints and vary in the tensile strength of the joints. These joints equally divide the entire block. The tensile strengths of the joints ( $\sigma$ ) are 0 MPa (T1 and T4), 4.39 MPa (T2 and T5) and 8.61 MPa (T3 and T6). The joints with different tensile strengths are defined by reducing the bond cohesion within the joint plane, while the joint planes have a width of 1.5 mm (3 times the mean size of particles) and a length of 45 mm (the same as the block's height). The joints with no tensile strength are simply defined by debonding the particles within the joint plane. Meanwhile, the block strength is unchanged (200.4 MPa) for all simulation conditions. With the design of pre-existing weak joints, rock block will break mainly along the weak joint planes at the initial stage of fragmentation during motion. Then the energy conversion of the block system and the variation in the motion of subblocks can be clearly recorded and analysed (here subblock represents the intact block cut by the pre-existing joint). The blocks with joints of no tensile strength (T1, T4) aim to represent the separation process of blocks that have been fractured, while the blocks that have joints with tensile strength are intended to simulate the blocks that cracking along joints and then separating. This point is very important for the following results and discussion. Note that the cracking of a rock block along specific directions or weak planes does not change the nature of rock fragmentation (Ghaffari et al., 2019). Instead of trying to replicate the complicated fragmentation processes that occur in real rock avalanches, the aims of this simplified configuration are to provide an opportunity to investigate the detailed microprocess of fragmentation and the effects of

fragmentation on a sliding-fragmenting rock mass system. Table A.1 in the appendix shows the main variables used in this study.

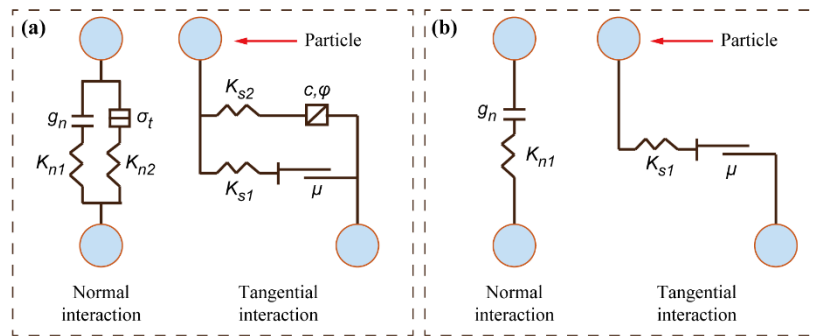


Figure 1: Schematic diagrams of the linear parallel bond model (a) and the linear model (b).

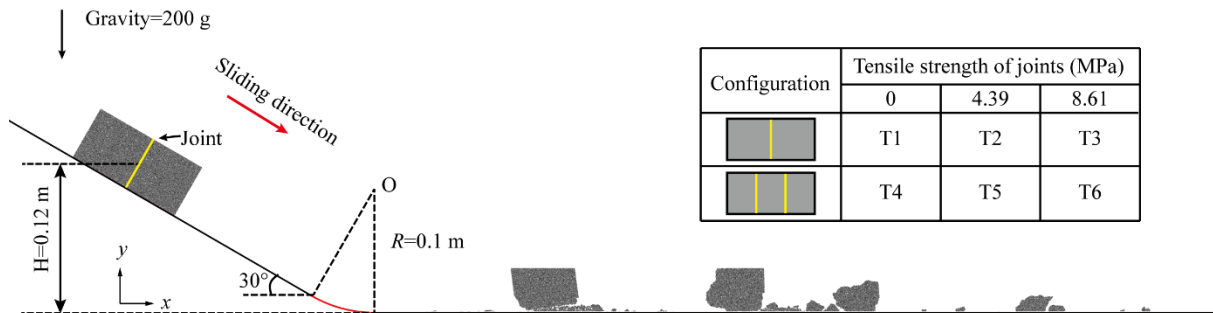


Figure 2: Schematic view of the model configuration. The detailed configurations of jointed rock blocks are shown in the inset table, and yellow lines in gray blocks represent the positions of joints. The joints with a width of 3 mm and a length of 45 mm equally divide the block.

**Referee comments:** *I also suggest to give a more detailed explanation concerning the relation between the number and spacing of fractures and the distance reached by blocks involved in the avalanche, since given explanation doesn't sound accurate enough.*

Thank you a lot for the useful comments and suggestions. The referee indicated that the given explanation of the relation between the number and spacing of fractures and the distance reached by blocks doesn't sound accurate enough. Actually, in that part of discussion, we attempted to discuss the relation between the strength of joint and the travel distance of fragments, which is still problematic. Thus, we detailed analyze the data, and trying to give a more robust explanation.

First of all, we found that the deposit figure of T6 is wrong, a small block run out of view. Therefore, we corrected that figure (Fig. 7).

Secondly, in order to detailed presents the deposit characteristics of rock block at different joint condition, we calculated the travel distance and degree of fragmentation of all simulations ( $L_t$  represents the travel distance of distal edge,  $L_{cm}$  represents the travel distance of the center of mass,

and  $F_d$  represents degree of fragmentation) (Fig. 8). Then, the deposit characteristics for all tests are discussed as follows:

Fig. 7 presents the final deposit features of all simulated conditions. Different colors represent the relative position of rock mass divided by joints. Rock mass mainly cracks along joints, and more intense fragmentation occurs within subblocks. It clearly shows that the frontal subblock presents higher degree of fragmentation than the middle and rear subblocks. Rock mass with two joints show higher degree of fragmentation in deposits compared to rock mass with one joint. Moreover, the deposits of all tests show good preservation of their initial rock mass sequence, which has also been reported in many natural rock avalanches (Heim, 1932; Strom, 2006; Hewitt et al., 2008; Dufresne et al., 2009).

Fig. 8 plots the travel distance and degree of fragmentation of rock mass at each test. We use the runout of the distal edge ( $L_t$ ) and the runout of the center of mass ( $L_{cm}$ ) to describe the travel distance of rock mass (Lin et al., 2020a). The relative breakage ratio ( $F_d$ ) is used to describe the degree of fragmentation (Hardin, 1985; Bowman et al., 2012). For one joint condition (T1, T2, and T3), with the increasing of joint strength, both runout of the distal edge ( $L_t$ ) and the runout of the center of mass ( $L_{cm}$ ) increase, so as the degree of fragmentation ( $F_d$ ). For rock mass with two joints condition, we can also see the increasing trend of travel distance (both  $L_t$  and  $L_{cm}$ ) and degree of fragmentation of deposits with joint strength, excepting for T5. As shown, T5 has less travel distance in both the distal edge and the center of mass, with higher degree of fragmentation. This difference may be due to the interaction of the fragments after initial fragmentation.

Thirdly, as shown by Figs. 7 and 8, T5 has different deposit characteristics. In the revised manuscript, we written that “As shown, T5 has less travel distance in both the distal edge and the center of mass, with higher degree of fragmentation. This difference may be due to the interaction of the fragments after initial fragmentation.” In our manuscript, we mainly discuss about the elastic strain energy variation induced by rock fragmentation, energy transfer induced by rock fragmentation and the multi-scale effects caused by rock fragmentation in rock avalanche. So the different deposit characteristics of T5 is not important enough and is comparative irrelevance. For this reason, we do not present detailed information to explain the formation of deposit of T5 in the revised manuscript. In the initial stage of fragmentation, T5 experiencing the “rotation back” of frontal subblock due to the interaction of fragments after the initial fragmentation stage. This “rotation back” movement increase the energy consuming of the interactions of fragments, and finally resulting in intense fragmentation and shorter travel distance of rock mass.

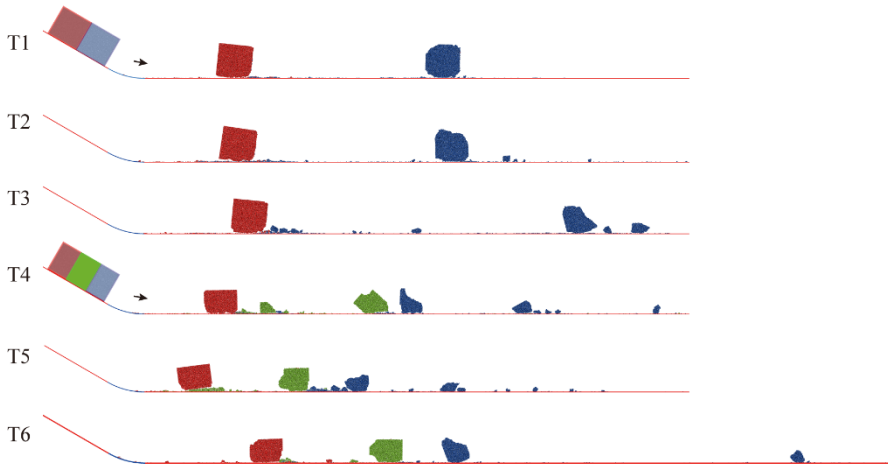


Figure 7: Deposit profiles of all simulations.

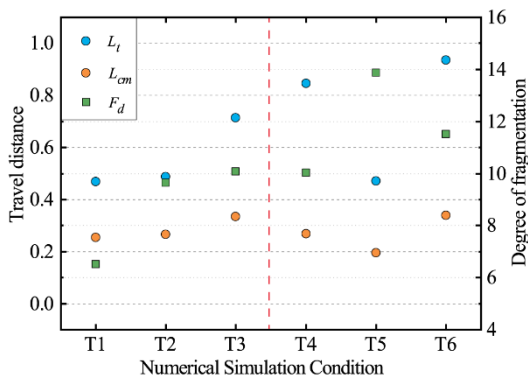


Figure 8: Travel distance and degree of fragmentation of all simulations ( $L_t$  represents the travel distance of distal edge,  $L_{cm}$  represents the travel distance of the center of mass, and  $F_d$  represents degree of fragmentation)

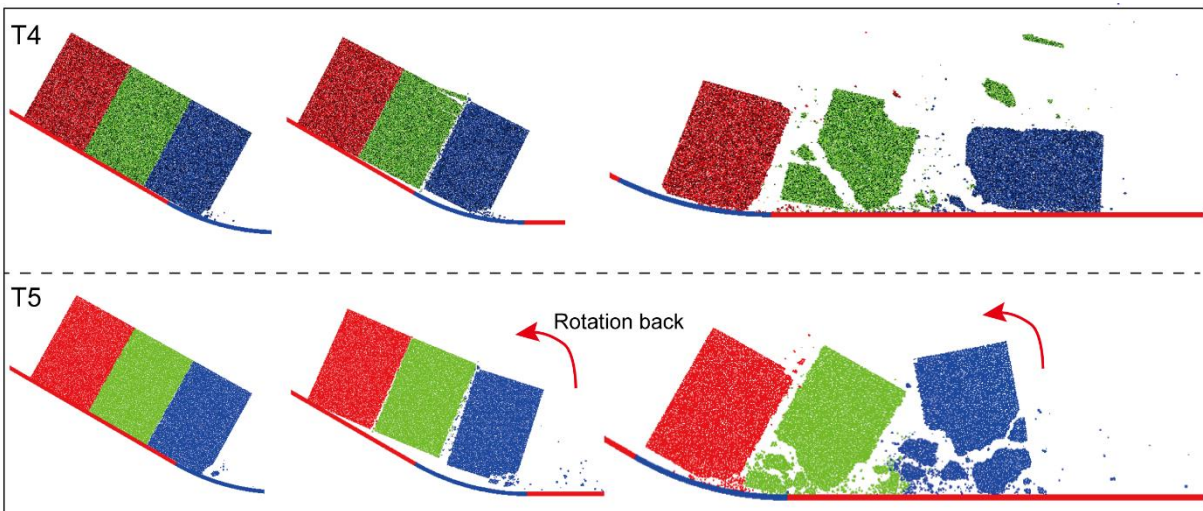
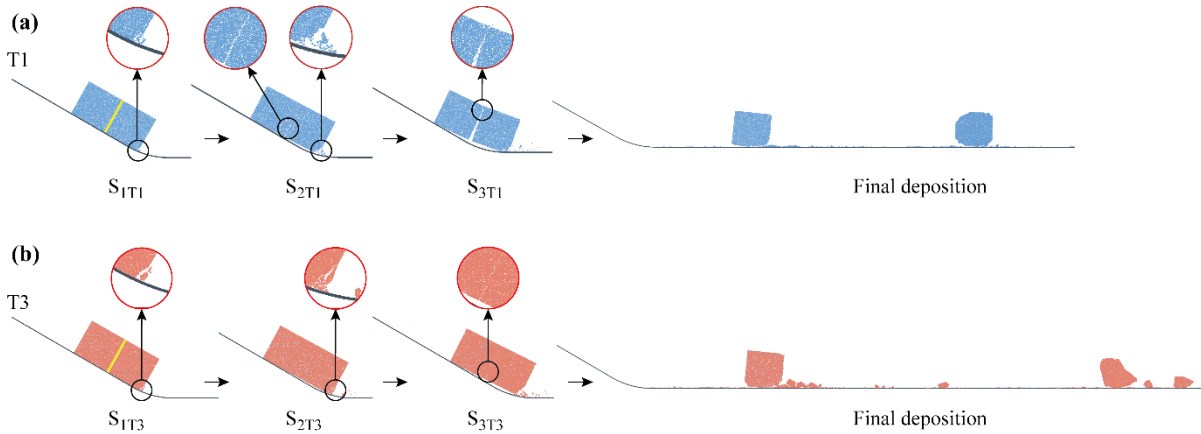


Figure R1: Fragmentation processes of T4 and T5

**Referee comments:** *Finally, figures' layout should be improved by applying a different colours palette and by indicating regressions equations and plots where available.*

Thank you very much for your useful comments. All the figures' layout indicated in the attached file are improved according to your suggestions. We presents these figures at following.



**Figure 3: (a) The evolution of T1 in the initial stage of fragmentation and its depositional characteristics. (b) The evolution of T3 in the initial stage of fragmentation and its depositional characteristics (S<sub>1T1</sub>, S<sub>2T1</sub>, S<sub>3T1</sub>, S<sub>1T3</sub>, S<sub>2T3</sub> and S<sub>3T3</sub> represent three specific stages/times for T1 and T3 that are described and analyzed later). The light blue subblock in the final deposition stage represents the rear part of the entire block, and the dark blue subblock represents the front part of the entire block.**

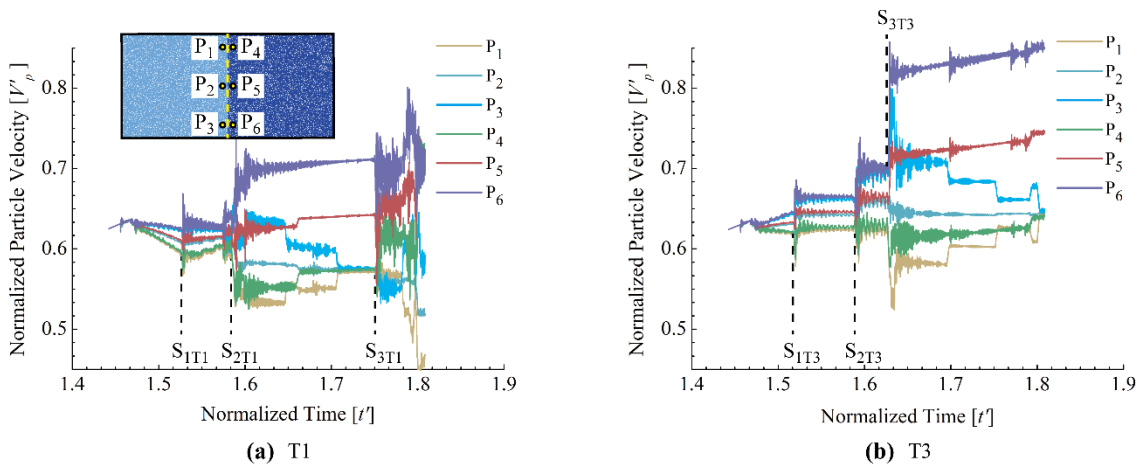


**Figure 4: (a) Normalized particle velocities of monitoring particles in T1 versus time (inset picture shows the relative positions of the six monitoring particles;  $t' = t / (2H/g')^{1/2}$ ;  $V'_p = V / (2g'H)^{1/2}$ ). (b) Normalized particle velocities of monitoring particles in T3 versus time.**

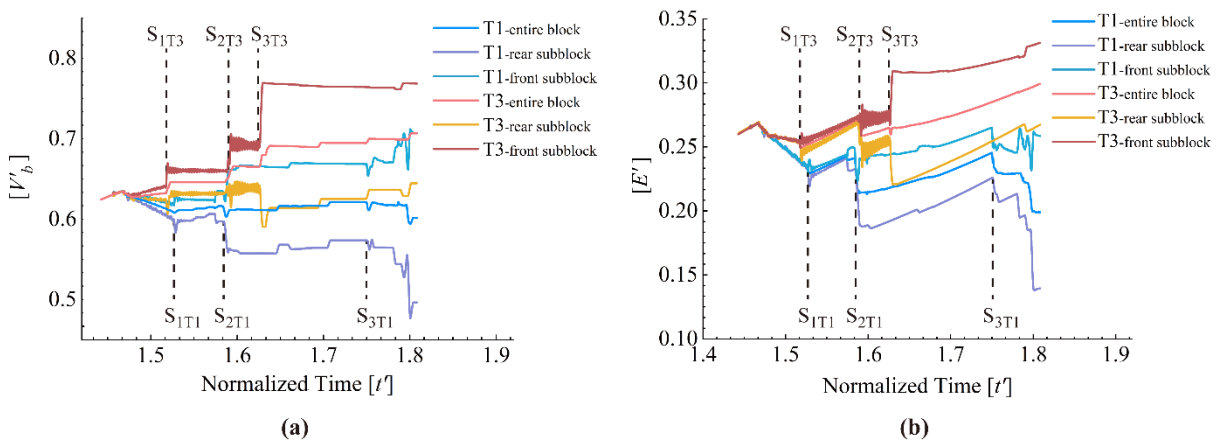


**Figure 5:** (a) The normalized horizontal velocities of blocks in T1 and T3 versus time ( $V'_b=V_b/(2 g'H)^{1/2}$ ). (b) The normalized kinetic energy evolution of blocks in T1 and T3 versus time ( $E'=E/mg'H$ ). Note that  $E'/2$  of the entire block is plotted.

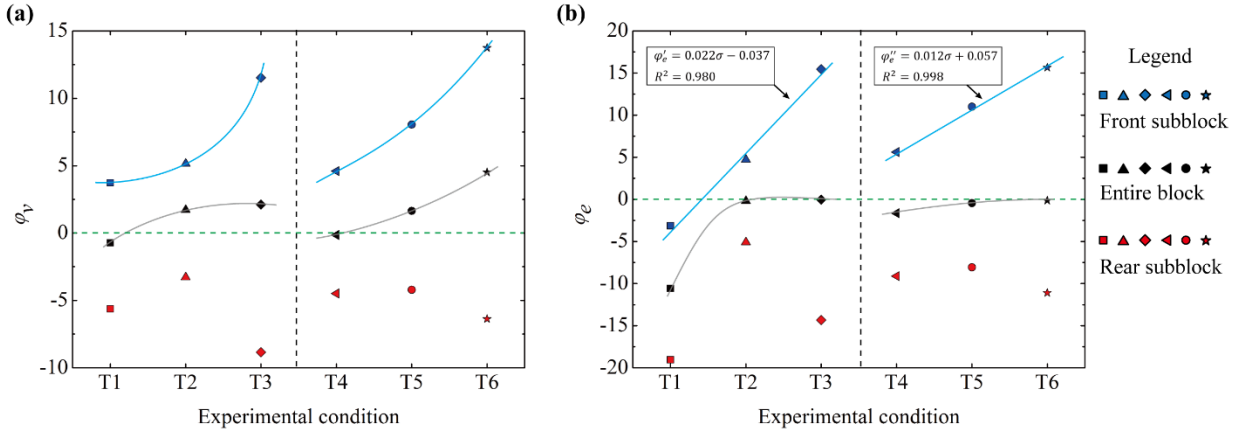


**Figure 6:** (a) The mean horizontal velocity incremental percentage ( $\phi_v$ ) and (b) the kinetic energy incremental percentage ( $\phi_e$ ) in the block separation stage for all tests.

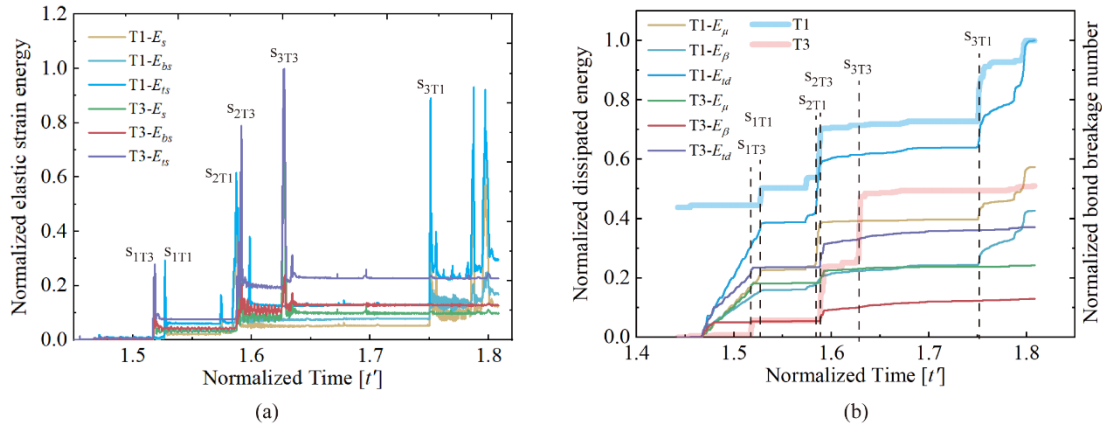


**Figure 9:** (a) The normalized elastic strain energy variation in the sliding block in T1 and T3 (normalized by the maximum total strain energy,  $E_{ts-max}$ ) versus time. (b) Normalized dissipated energy variation in the sliding block in T1 and T3 (normalized by the maximum total dissipated energy,  $E_{td-max}$ ) versus time. The two bold curves represent bond breakage number variations (which are also normalized by the maximum bond breakage number) of T1 and T3 versus time.